metals

MDPI

Article

Effect of Heat Treatments on Microstructure and Mechanical Properties of Low-Cost Ti-6Al-4V Alloy Produced by Thermomechanical Powder Consolidation Route

Ajit Pal Singh [1,*], Rob Torrens [1], Brian Gabbitas [1] and Giribaskar Sivaswamy [2]

[1] Waikato Centre for Advanced Materials and Manufacturing (WaiCAMM), University of Waikato, Hamilton 3240, New Zealand
[2] Advanced Forming Research Centre (AFRC), University of Strathclyde, Glasgow PA4 9LJ, UK
* Correspondence: ajitpal.singh@waikato.ac.nz or ajit-pal-90@hotmail.com; Tel.: +64-7-262-0533

Abstract: This paper investigates the level of properties enhancement achievable by heat-treating Ti-6Al-4V alloy produced from a blended powder mixture using a thermomechanical powder consolidation route involving warm uniaxial pressing and vacuum sintering followed by extrusion at super transus temperature (1150 °C). The as-extruded material with a higher oxygen content of 0.55 wt.% was subjected to two different sub-transus annealing treatments: HT-A: 955 °C/1 h-furnace cooling and HT-B: 925 °C/4 h-cooling @ 50 °C/h to 760 °C-furnace cooling. Room temperature Charpy v-notch impact toughness tests and tensile tests were performed to ascertain the effect of microstructural changes during post-extrusion annealing treatments. After impact tests, analysis of microstructures and fracture surfaces of samples was carried out using optical and scanning electron microscopy. The as-extruded material displayed mean impact toughness of 4 J along with a yield strength of 956 MPa, an ultimate tensile strength of 1150 MPa, and an elongation to fracture of 2.4%. The annealing treatments gave a noticeable enhancement in the impact toughness (average values 5–6 J obtained) while maintaining a yield strength and ultimate tensile strength level of about 992 MPa and 1164–1181 MPa, respectively. Additionally, the level of change in ductility was limited for each sub-transus annealing treatment, and HT-A has given only a 30% increase compared to as-extruded material.

Keywords: titanium alloys; thermomechanical powder consolidation; microstructures; impact toughness; tensile properties; crack propagation; fracture behaviour

Citation: Singh, A.P.; Torrens, R.; Gabbitas, B.; Sivaswamy, G. Effect of Heat Treatments on Microstructure and Mechanical Properties of Low-Cost Ti-6Al-4V Alloy Produced by Thermomechanical Powder Consolidation Route. *Metals* **2023**, *13*, 173. https://doi.org/10.3390/met13010173

Academic Editor: Frank Czerwinski

Received: 4 December 2022
Revised: 11 January 2023
Accepted: 12 January 2023
Published: 14 January 2023

1. Introduction

Titanium and its alloys are vital for future developments due to their high strength-to-weight ratio, remarkable corrosion resistance, high toughness, good resistance to fatigue, excellent biological compatibility, and the ability to withstand moderately high temperatures without creep [1–4]. Titanium alloys have found a wide range of applications in many industries aerospace, power generation, chemical processing, heat exchangers, medical applications, sports, and automotive. However, the high production cost of titanium is a significant obstacle restricting its widespread use in everyday applications. Titanium parts manufactured by ingot metallurgy cost approximately four times more than their steel counterparts [2]. Therefore, there is a great impetus to explore alternative manufacturing routes that can offer higher levels of material utilisation through near-net shape processing coupled with minimum machining.

Powder metallurgy (PM) is one such technique that avoids costly melt processes and shorter procurement lead times. It increases the utilisation of the material to 95%, resulting in an estimated 20–50% cost savings compared to conventional parts [5]. Besides the economic efficiency, PM can produce complex shape parts with a high degree of freedom in

the selection of alloy composition and resulting in desired uniform microstructure characteristics. Many established PM methods exist for consolidating metal powders [6–13]. Thermomechanical powder consolidation (TPC) processes (such as powder extrusion and forging) are a natural extension of the conventional press and sinter process. Here, the desired final shape of the part is obtained from extrusion or forging procedure using sintered compacts. During TPC processes, particles in the powder compact plastically deform to offer several advantages, including the elimination of pores present after sintering, refinement of grain size, and deformation of the prior particle surfaces. The deformation causes a change in particle shape to fill the gaps better and assist the joining of particles by creating new particle surfaces. Therefore, the resulting final part is fully dense and has unique microstructure and mechanical properties [14–16].

Ti-6Al-4V is the most commonly used alloy, accounting for more than 50% of total titanium usage worldwide and therefore referred to as the workhorse of the industry [2]. Ti-6Al-4V alloy is an excellent candidate for aerospace applications due to its mechanical properties, which can be altered by changing processing conditions or with appropriate heat treatment [2,17]. The mechanical properties can be controlled by refining the amount and distribution of α and β phases [17]. Typical tensile properties of the grade five Ti-6Al-4V alloy can range between 800–1100 MPa yield strengths and 896–1200 MPa ultimate tensile strength, while the material's ductility varies between 10–16% [2,17]. Unlike the extensive discussion and analysis on the static properties of Ti-6Al-4V alloy [2,13,18,19], there is little discussion in the literature on the dynamic properties, including the impact properties of PM-produced Ti-6Al-4V alloy. Many applications for these powders produced titanium materials where fracture-related properties such as impact properties and fracture toughness are essential. Due to this reason, a broad spectrum of available literature values of the impact energy is included in this section to assess the Ti-6Al-4V alloy performance at high strain rates [20–25]. From Figure 1, it is clear that Extra Low Interstitial (ELI) ingot Ti-6Al-4V alloy can have impact energy values in the range of 24~40 J, and standard grade five Ti-6Al-4V alloy can achieve toughness 20~27 J.

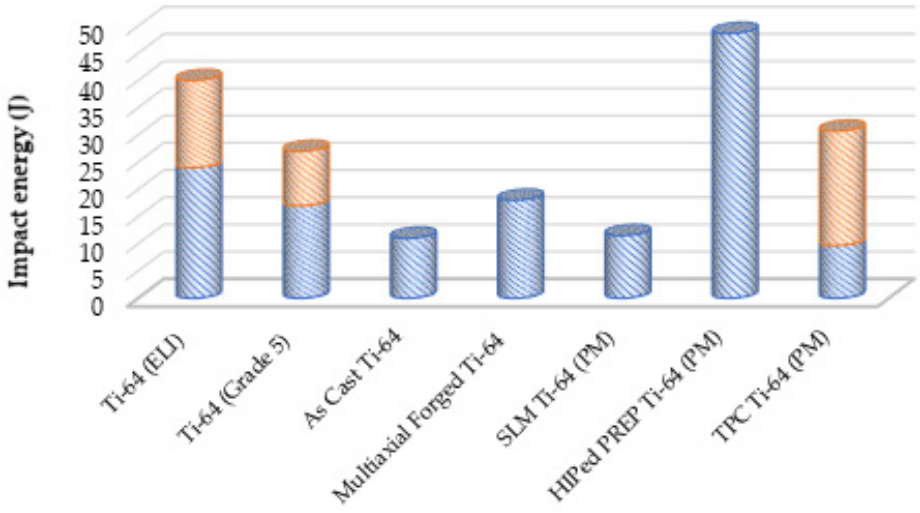

Figure 1. Impact toughness (range) of Ti-6Al-4V alloy produced by various ingot and PM methods [20–32].

According to the studies by Zherebtsov et al. and Reda et al., the impact toughness of as-processed Ti-6Al-4V alloy by casting and multi-axial forging can be 11 J and 18 J, respectively [23,24]. Regarding PM-produced Ti-6Al-4V alloy, hot isostatically pressed PREP powder can provide superior impact energy of around 48 J compared to ingot or other PM routes such as SLM [21,22]. The significant research performed by the author on Ti-6Al-4V alloy fabricated using the TPC route reveals that impact toughness in the range of 9.7–21 J can be achieved depending on the level of oxygen impurity contents and

type of heat treatments employed [28–32]. Generally, low impurity content and optimized microstructures result in high-impact toughness. Meyer et al. showed that furnace cooling of the material from 955 °C is an effective way to enhance the impact properties of a mill-annealed wrought Ti-6Al-4V alloy [33].

In the literature, it is reported that sub-transus annealing treatments of TPC-produced Ti-6Al-4V alloy can achieve lamellar type microstructures with desirable grain, colony, lamellar α, and grain boundary α morphology to enhance the fracture-related properties despite the presence of high oxygen impurity (0.33–0.42 wt.%) in the material [30,31]. Oxygen is an α stabilizer that increases the β transus temperature and promotes the formation of α precipitates during subsequent cooling [2]. No study in the literature provides impact data for powder-produced Ti-6Al-4V alloy with oxygen impurity contents above 0.43 wt.%. Therefore, the effectiveness of these sub-transus annealing on PM-produced Ti-6Al-4V alloy with extremely high impurity contents is still unknown. The focus of the current study is to determine the level of mechanical properties obtainable through sub-transus annealing treatments (955 °C/1 h-furnace cooling and 925 °C/4 h-cooling @ 50 °C/h to 760 °C-furnace cooling) for Ti-6Al-4V alloy which contains 0.55 wt.% oxygen impurity and produced using TPC route.

2. Materials and Methods

The nominal composition Ti-6Al-4V was obtained by blending the 9:1 weight ratio of elemental hydride-dehydride (HDH) titanium powder and master alloy powder (MA-60 wt.%.Al-40 wt.%V). The measured oxygen impurity contents and particle size of these starting powders are displayed in Table 1. A three-stage roller mixing approach was deployed to blend 5 kg raw powders homogeneously without a suitable capacity powder mixing equipment. During the first stage, ten separate batches containing 500 g of powder mixture with stainless steel balls (2:1 weight ratio to powder) were added to an airtight plastic container to assist in the blending process. A roller mill was used to rotate this container at a speed of 200 rpm for 24 h. After completing the mixing cycles, the compositional homogeneity of these individual mixes was further enhanced by adding five of these 500 g mixes into a large capacity airtight plastic container. Two batches containing 2500 g of powder mixed with an appropriate volume of stainless-steel balls were again milled for 24 h using the same speed and roller mill. For the final mixing stage, the powder mixture from both batches was transferred to a new larger container after sieving the stainless-steel balls. This container was manually stirred for sufficient time to achieve a single Ti-6Al-4V powder batch of five-kilogram quantity.

Table 1. Particle size and oxygen impurity content of starting powders.

Start Materials	HDH Titanium	Master Alloy (Al60-V40)
Particle size	−200 mesh	−250 mesh
Mean particle size (d_{50})	51.25 μm	35.88 μm
Oxygen impurity content (wt.%)	0.23~0.25	0.61~0.67

The blended powder mixture was consolidated using the sequence of thermomechanical processing operations schematically illustrated in Figure 2. The uni-axial warm compaction of the blended powder mixture was performed at 260 °C in air, with a compaction pressure of 450 MPa. The inner surface of the compaction die and plunger were coated with colloidal graphite lubricant to reduce die-wall friction. The resulting green cylindrical powder billet had a diameter of 102 mm and a height of 148 mm. Based on these dimensions and its mass, the relative green density of the billet was calculated to be between 84–86%. To perform the final extrusion of the green billet in the air, it had to have further consolidation using vacuum sintering (to get a relative density of ~93%). The sintering was performed using a commercial scale vacuum furnace ZSJ—35 × 35 × 70 (manufactured by Advanced Corporation for Materials & Equipments Co. Ltd. (ACME),

MuYun Industrial Zone, Changsha, China). The four-step sintering cycle was adopted. In the first step, the green billet was heated to 260 °C at a heating rate of 10 °C/min. Step two was an isothermal hold of 6 hrs to achieve a high vacuum, in the range of 1–3 × 10^{-2} Pa. Step three involves heating billet at a heating rate of 10 °C/min to 1400 °C. In the final step, the isothermal hold time was selected to be 3 h, followed by natural furnace cooling (FC) to room temperature. For hot extrusion, the vacuum-sintered billet was heated to a temperature of 1150 °C using an induction coil in air. A protective layer of high-temperature glass was applied to the surface of the vacuum-sintered billet to prevent oxidation before extrusion. The hot billet was manually shifted to a well-lubricated cylindrical extrusion chamber, which along with the die, was already at 420 °C. The ram of a 700-ton vertical hydraulic press was used to push the billet through a rectangular profile extrusion die, with a cross-sectional area that resulted in an extrusion ratio of 9:1. As-extruded bar had a cross-sectional dimension of 36 mm (W) × 16 mm (H) and a length (L) of 1000 mm.

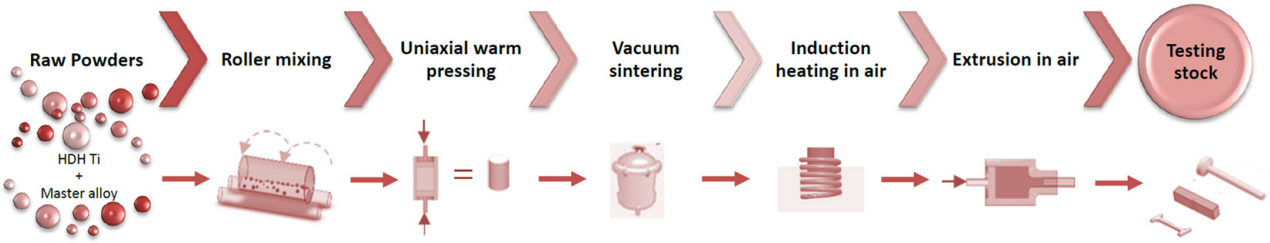

Figure 2. The sequence of operations used to prepare the Ti-6Al-4V alloy bar using a combination of warm compaction, vacuum sintering, and a blended powder mixture extrusion.

The material characteristics, including actual chemical composition and oxygen impurity contents of as-extruded material, were obtained by X-ray fluorescence (Spectro Xepos spectrometer, SPECTRO Analytical Instruments, Kleve, Germany) and LECO inert gas fusion method, respectively. The processed rectangular bar was cut into multiple appropriate lengths, and the oxygen-enriched outer α-case layer from each section was machined off before the post-extrusion annealing treatments. In the first sub-transus annealing treatment 955 °C/1 h-FC (now onward referred to as HT-A), the material was heated to 955 °C followed by a one-hour isothermal hold. It was then furnace cooled to room temperature. The second sub-transus heat treatment (925 °C/4 h-cooling @ 50 °C/h to 760 °C-FC) consisted of annealing at 925 °C for 4 h, followed by a controlled furnace cooling at a cooling rate of 50 °C/h to 760 °C, then natural furnace cooling to room temperature. This condition will be referred to as HT-B.

The selected sub-transus annealing temperature (925–955 °C) and isothermal holding time are designed to adjust the α volume fraction. In contrast, the cooling rate and secondary cooling stage to 760 °C is selected to change the width and length of α lamellae substantially. Both heat treatments were performed in a vacuum furnace (ACME, ZSJ—20 × 20 × 30) (Advanced Corporation for Materials & Equipments Co. Ltd. (ACME), MuYun Industrial Zone, Changsha, China). The microstructures of as-extruded along with heat-treated material were observed using an optical microscope (Olympus BX60, Olympus Optical Co Ltd, Tokyo, Japan) and a scanning electron microscope (SEM) (Hitachi S-4700, Tokyo, Japan). The ground and polished samples for optical and SEM were etched in a modified Kroll's reagent consisting of 2 vol.% HF, 4 vol.% HNO_3, and 94 vol.% H_2O.

Multiple flat dog-bone-shaped tensile test specimens with a square cross-section of 1.8 × 1.8 mm and a gauge length of 20 mm were prepared from longitudinally orientated material. Tensile testing was carried out at room temperature using an Instron 4204 universal machine (Instron, Norwood, MA, USA). The strain was measured using a clip-on extensometer with a gauge length of 10 mm, and tests were done using a strain rate of 1 × 10^{-4} s^{-1}.

The high strain rate performance data for the material under a tri-axial stress state was obtained using standard Charpy impact specimens with dimensions 10 mm × 10 mm × 55 mm

were machined, and a 2 mm deep v-notch (with an approximate tip radius of 0.25 mm) was introduced as specified in the ASTM standard E23-07. Impact testing was performed at room temperature using an Avery-6703 impact tester (Avery Denison, United Kingdom) with a maximum energy rating of 300 J, an impact velocity of 5 m/s, and a margin of error of ±2 J. The fracture surfaces of impacted specimens were examined using a Zeiss Evo MA25 SEM (Jena, Germany). Additionally, an impact specimen tested in the as-extruded and each heat-treated state were sectioned longitudinally (perpendicular to the crack propagation direction) to study the crack propagation mechanism. The samples attained in this manner were cold-mounted using a vacuum impregnation system using self-curing epoxy resin before mechanical grinding, polishing, and etching with Kroll's reagent. An Olympus BX60 (Olympus Optical Co Ltd, Tokyo, Japan) optical microscope was used to examine the microstructural features present along the crack path.

3. Results and Discussion

A blended elemental approach is very attractive for obtaining the desired alloy composition at a relatively low cost. However, creating an alloy with a homogeneous composition can be challenging, especially when large quantities of pure titanium and master alloy powders are blended. Detailed information about the material's chemical composition, homogeneity, impurity content, oxygen impurity pick-up, microstructural variations, and tensile properties along the length of the as-extruded Ti-6Al-4V rectangular bar utilised in the current study has been published previously [34]. The elemental concentrations of the as-extruded material displayed in Table 2 are within the specifications stated in the ASM standard (aluminium and vanadium are between 5.5–6.75 wt.% and 3.5–4.5 wt.% respectively) [27]. The oxygen impurity content of as-extruded Ti-6Al-4V alloy is 0.55 wt.% which is exceptionally higher than standard ingot grade five Ti-6Al-4V alloy (0.2 wt.%), and the impurity level acceptable for PM-produced structural components in accordance to ASTM-B988 [27,35]. The oxygen impurity pick-up mainly occurred during vacuum sintering of the 5 kg green billet, which is at least four times higher than the processing of a standard lab-scale 500 g powder compact [34]. This highlights that scaling up the powder extrusion process to produce Ti-6Al-4V alloy on an industrial scale is not straightforward, and processing large quantities of blended powder imposes various challenges. The following section explores the general morphology of the microstructures attained after extrusion and two different sub-transus annealing treatments.

Table 2. Measured chemical composition and oxygen content of the extruded Ti-6Al-4V bar.

Material	Composition [wt.%]			
	Ti	Al	V	O
As-extruded Ti-6Al-4V	90.65	5.60	4.25	0.55

3.1. Microstructural Characteristics of As-Extruded Bar

Microstructural analysis of the as-extruded bar using an optical microscope revealed equiaxed β grains with lamellar α as shown in Figure 3. The severe deformation during extrusion and air cooling had restricted the growth of the recrystallized β grains, and a microstructure with much smaller α colonies containing finer α lamellae had formed. The formation of a continuous α layer along the grain boundaries of most of the prior β grains can also be observed. The β grains of the extruded bars have a typical size of about 140 µm along with an α-colony size of about 50–60 µm.

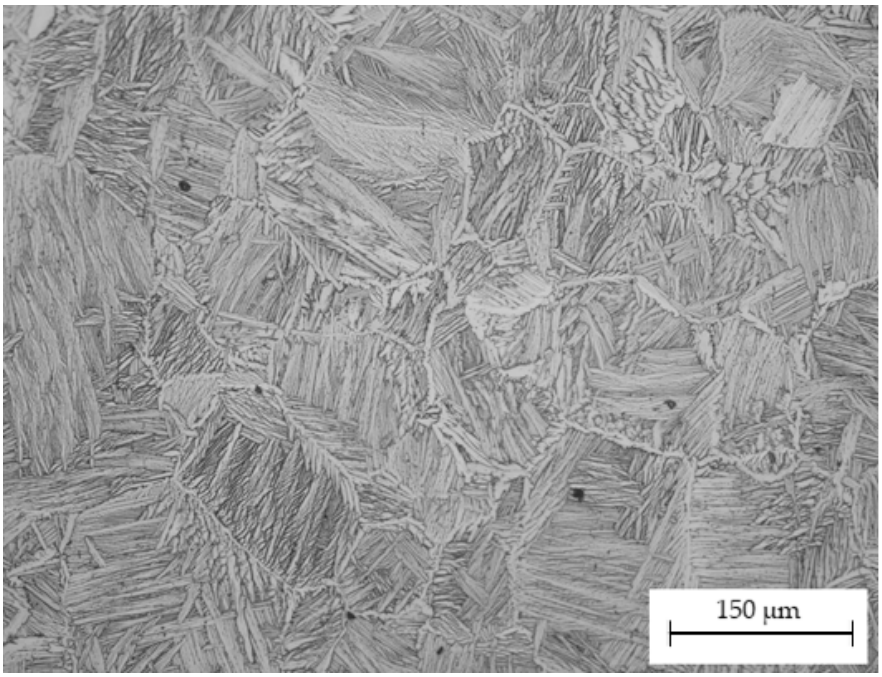

Figure 3. Optical micrograph showing a typical lamellar/Widmanstätten type structure of Ti-6Al-4V alloy attained after air cooling from β phase field.

3.1.1. Microstructure after HT-A Heat Treatment

This sub-transus annealing treatment resulted in a fully homogenous lamellar microstructure within the β grains and a well-developed α phase at the β grain boundaries. The relatively slow furnace cooling from 955 °C caused a significant increase in the α lamellar thickness. In contrast, other aspects of the microstructure: α lamellae length, prior β grain size, colony size, and α grain boundary layer, were little changed compared with a microstructure produced by prior thermomechanical processing (see Figure 4a,b). Most of the β grains covered by the area shown in the micrograph had a size between 130–160 µm. The volume fraction of α phase in this particular microstructure is estimated to be 95.8%.

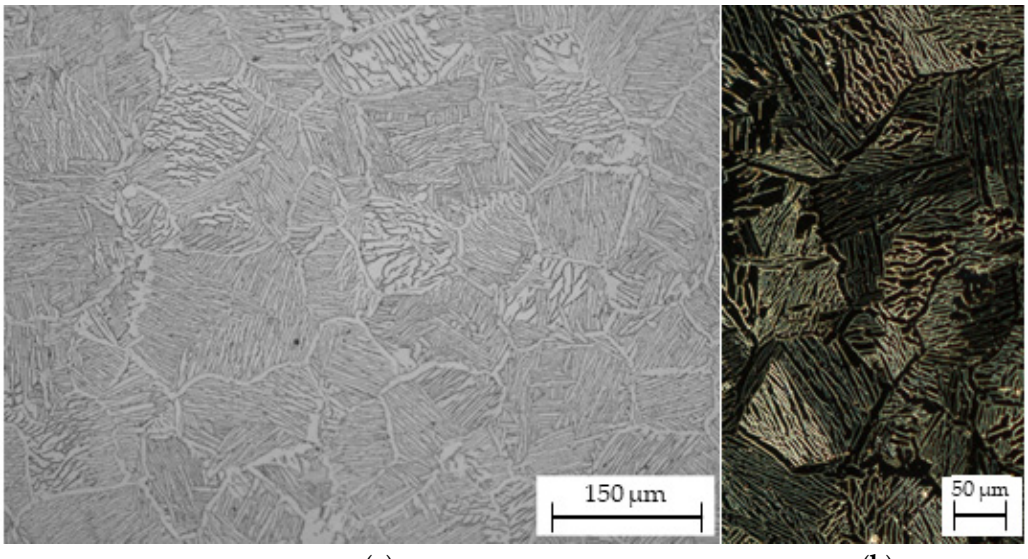

(**a**) (**b**)

Figure 4. Fully lamellar microstructure attained after HT-A (furnace cooling from 955 °C) (**a**) overall appearance (**b**) morphology of individual α platelets and retained β phase matrix.

3.1.2. Microstructure after HT-B Heat Treatment

The microstructure after the HT-B heat treatment, where the material was kept at 925 °C for 4 h, cooled at 50 °C/h to 760 °C, then furnace cooled, has a complex colony arrangement containing partly broken up β lines distinguishing each lenticular lamellar plate, as shown in Figure 5a,b. An estimation of the size of microstructural features suggests prior β grains of mean size ~140 ± 14 µm and a range in α/β colony size of 55–65 µm. It is estimated that this microstructure has 97.6% volume fraction of α phase. Understandably, that very slow and controlled cooling from 925 °C to 760 °C at a rate of 50 °C/h, followed by standard furnace cooling, was responsible for a coarsening of the α phase. Overall the morphology of this microstructure does match the microstructure described, where the same heat treatment was employed on material containing relatively low oxygen impurity and produced using the laboratory scale extrusion setup (20 mm diameter rods). Figure 5b illustrates the few areas in this microstructure that contain complex triple joints and discontinuous grain boundaries.

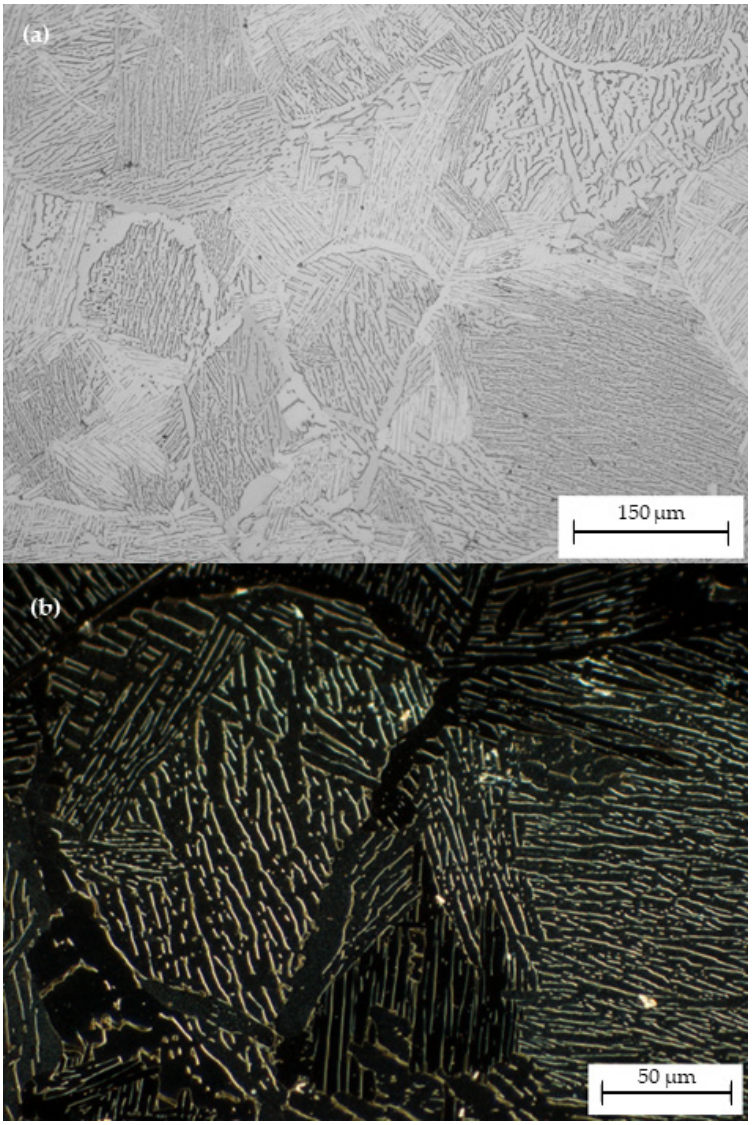

Figure 5. Micrographs showing equiaxed β grains with colonies of α and lamellarα developed after HT-B (925 °C/4 h-@50 °C/h to 760 °C-FC) (**a**) Low magnification micrograph from the optical microscope (**b**) dark field image showing the distribution of β phase.

3.2. Tensile and Impact Properties

This section presents the room temperature tensile properties derived from 1.8 × 1.8 mm cross-section and 20 mm gauge length micro-tensile specimens tested at a strain rate of 1×10^{-4} s^{-1}, along with impact toughness determined from Charpy v-notch specimens as per ASTM standard E23-07.

3.2.1. Tensile Properties

The insignificant effects of heat treatment on the strength and ductility of extruded Ti-6Al-4V bar can be visualised in Table 3 and Figure 6. It should be noted that the tensile results reported here are the mean values based on three replicate tests for each condition. According to the ASM standard, commercial Ti-6Al-4V alloy (oxygen impurity content: <0.2 wt.%) is expected to have yield strength of 880 MPa, ultimate tensile strength (UTS) of 950 MPa, and an elongation to fracture of about 14% [27]. The strength values displayed by the Ti-6Al-4V alloy bar produced in this study are 75–230 MPa higher, whereas the ductility is significantly lower (only 20% of the expected value for material produced by ingot metallurgy). The superior strength and poor ductility values could be linked to a significantly higher oxygen content (0.55 wt.%) leading to microcracks in relatively fine microstructure deriving from a TPC process [34].

Table 3. Summary of average tensile properties obtained for as-extruded and annealed Ti-6Al-4V alloy prepared from blended powders using thermomechanical powder consolidation (TPC) route.

Sample	Yield Strength (MPa)	Ultimate Tensile Strength (MPa)	Elongation to Fracture (%)
As-extruded (AE)	956 ± 30	1150 ± 97	2.4 ± 0.7
HT-A	993 ± 12	1181 ± 44	3.2 ± 0.5
HT-B	992 ± 11	1164 ± 22	2.3 ± 0.5

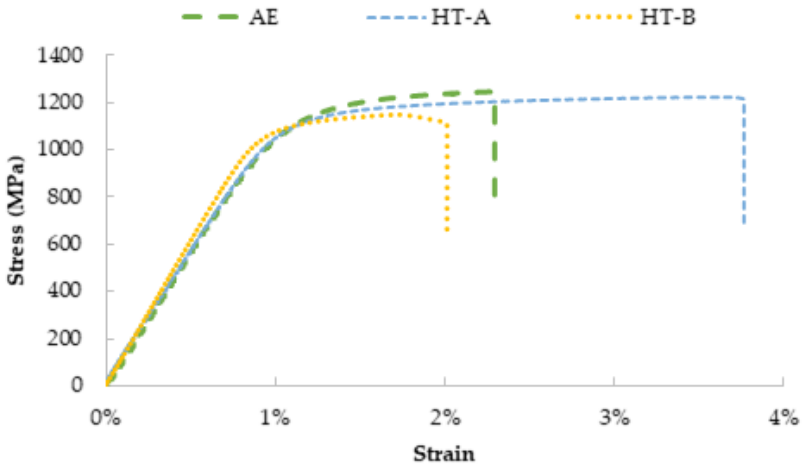

Figure 6. Typical stress and strain curves of as-extruded and heat-treated Ti-6Al-4V alloy produced using thermomechanical powder consolidation (TPC) route.

The as-extruded bar had a yield strength of 956 MPa, a tensile strength of 1150 MPa, and an average elongation to fracture of 2.4%. HT-A heat treatment consisted of furnace cooling from 955 °C, which gave a relatively high yield strength and UTS of 993 MPa and 1181 MPa, respectively, and a slightly improved ductility (elongation to fracture of 3.2%). On the other hand, HT-B heat treatment (925 °C/4 h-@50 °C/h to 760 °C-FC) resulted in a reduction in elongation to fracture (2.3%), whereas the change in yield strength (992 MPa) and UTS (1164 MPa) was minimal after considering the standard error associated with each data set.

The change in strength and ductility after each heat treatment can be explained in terms of variations in microstructure, particularly the morphology and size of primary α (lamellar) and the size of β grains formed within the matrix. Generally, the bcc β phase offers more slip systems than the hcp α phase [36]. Figures 4 and 5 shows that the volume fraction of the β phase in the HT-A microstructure is higher than that after heat treatment HT-B. In the HT-A microstructure, individual α lamellae were well surrounded by a continuous and relatively thick β phase, whereas the thickness and continuity of the β matrix after heat treatment HT-B were lower. Therefore, a slightly higher ductility would be expected after heat treatment HT-A. The values of failure stress attained for each case closely matched the UTS of the material, as shown in Figure 6. This shows that localised necking occurs immediately after diffusion necking during tensile testing, leading to fracture.

In summary, a relatively high oxygen impurity content of 0.55 wt.% in as-extruded material plays a favourable role in strengthening the alloy. Interstitial oxygen atoms occupy octahedral sites of the hcp α-phase crystal structure and increase the lattice parameters along with the c/a ratio in the crystal [37,38]. Therefore, oxygen solute atoms interact with the hydrostatic fields of both edge and screw dislocations to reduce dislocation mobility, increasing the material's strength [37–39]. A general variation in microstructural features (particularly change in α/β phase fraction) does not enhance the ductility much, even after heat-treating extruded material. The main reason for this could be a relatively unchanged lamellar α morphology, which remains coarse. The continuous β grain boundary α phase formed after sub-transus annealing may have also adversely affected ductility.

3.2.2. Impact Toughness

The average impact energy values for three replicate test specimens, prepared from as-extruded and heat-treated sections of a Ti-6Al-4V alloy bar, are shown in Figure 7. The Charpy impact toughness of a Ti-6Al-4V alloy bar in the as-extruded condition was 4 J. After heat-treatment HT-A (955 °C/1 h-FC), the impact energy was slightly improved, and an average value of 6 J was attained. After heat treatment HT-B (925 °C/4 h-@50 °C/h to 760 °C-FC), the impact energy was 1 J higher than that for the as-extruded material and slightly lower than that given by the HT-A sample. This increase in impact toughness after heat treatment was mainly attributed to a coarsening of the α lamellar morphology that occurred during the relatively slow cooling from temperature maintained in the α + β regime.

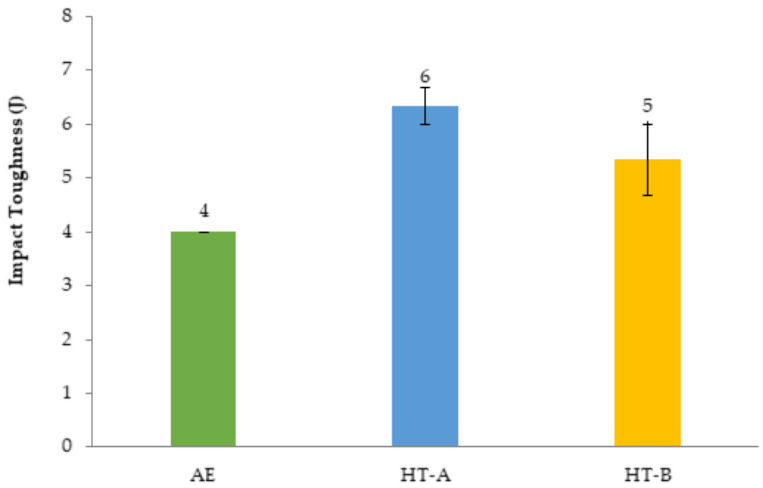

Figure 7. Histogram showing the variation in the Charpy impact toughness values of Ti-6Al-4V alloy in the as-extruded condition and after two different heat treatments.

It has already been described in [31] that a coarser microstructure provides an exceptionally tedious crack path, and as a result, a crack tip has to follow a complex and long zig-zag path. Hence, the overall impact toughness has increased after HT-A.

3.3. Fracture Behaviour during Charpy Impact Testing

This segment explores a possible relationship between microstructure and fracture behaviour of impact test specimens through an investigation of the crack path and an in-depth examination of fracture surfaces.

3.3.1. Fracture Surfaces

The fracture surfaces of broken Charpy impact specimens are shown in Figure 8. From these SEM fractographs, it is clear that brittle fracture was the predominant failure mode. Generally, an indication of ductile fracture behavior is manifested by pronounced shear lips. In this study, only HT-A heat-treated material showed minor signs of shear lip formation at high magnification.

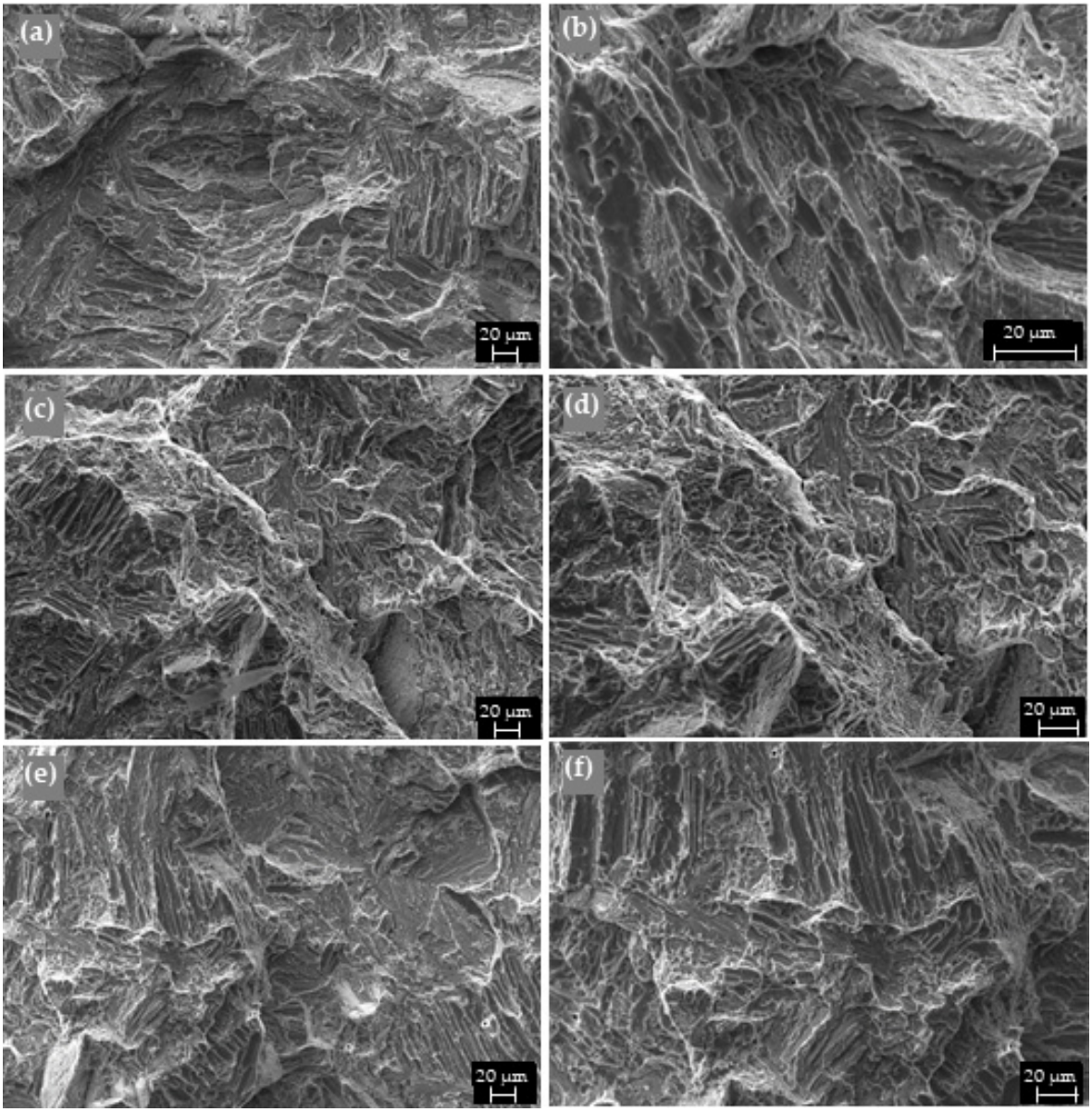

Figure 8. Fractographs of Charpy impacted specimens of Ti-6Al-4V alloy (**a**,**b**) as-extruded (**c**,**d**) HT-A heat treated (**e**,**f**) HT-B heat treated.

Additionally, in this particular case, the general roughness and irregularity of the fracture surface were significantly high, along with the signs of ductile dimples (Figure 9). This kind of observation highlights the fact that this particular heat treatment gives a microstructure that provides more resistance to crack propagation compared to as-extruded and HT-B condition samples, where relatively large transgranular features were evident.

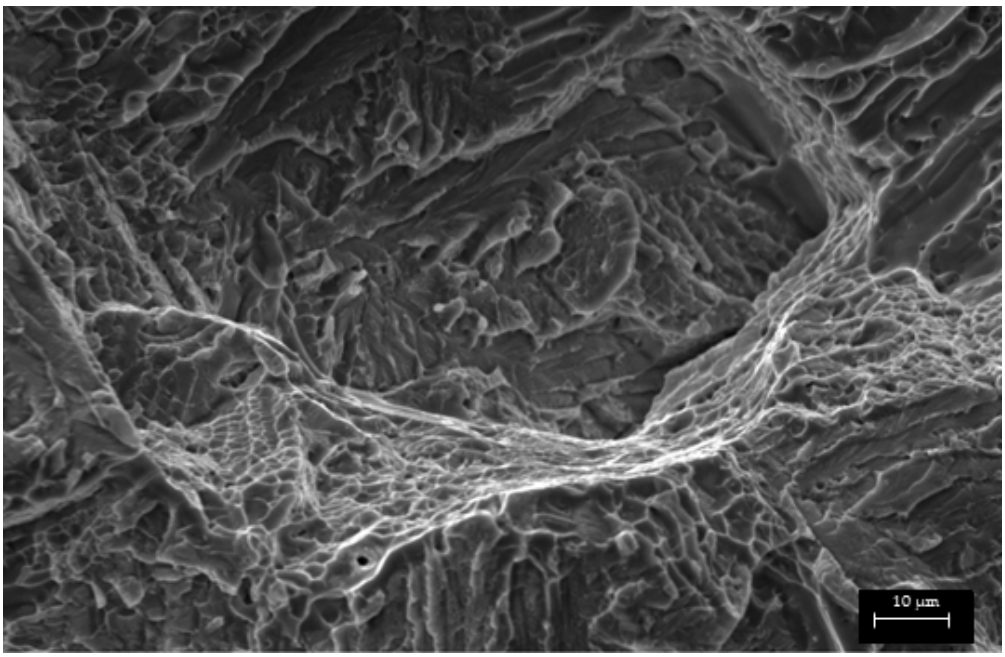

Figure 9. SEM fractographs showing the presence of ductile dimples in HT-A impact toughness specimen.

3.3.2. Crack Propagation Behaviour

To further justify that enhancement in impact toughness occurred due to crack tortuousness, the crack propagation path in each of the individual cases was analysed by recording micrographs along the crack path (Figure 10). These micrographs clearly show that each microstructure played a role in causing frequent changes in the path of crack propagation. However, the fracture profiles indicate that the degree of deflection or zigzagging of the crack front in the material given heat treatment HT-A was relatively large (compare Figure 10a,c,e). This observation supports the finding that the crack has done much work to break the specimen in this particular case. As a result, relatively high impact toughness was obtained compared to as-extruded and HT-B heat-treated materials.

In terms of the crack propagation route, crack spread through the interior of grains, and the α colony boundary interfaces provided significant resistance to crack propagation in each case (Figure 10b,d,f). In the case of heat-treated material, resistance to crack propagation was also influenced by a combination of features such as a thick grain boundary α layer, individual α lamellae, and a retained β phase matrix. Overall, no sign of crack branching or secondary cracking was observed in these three cases.

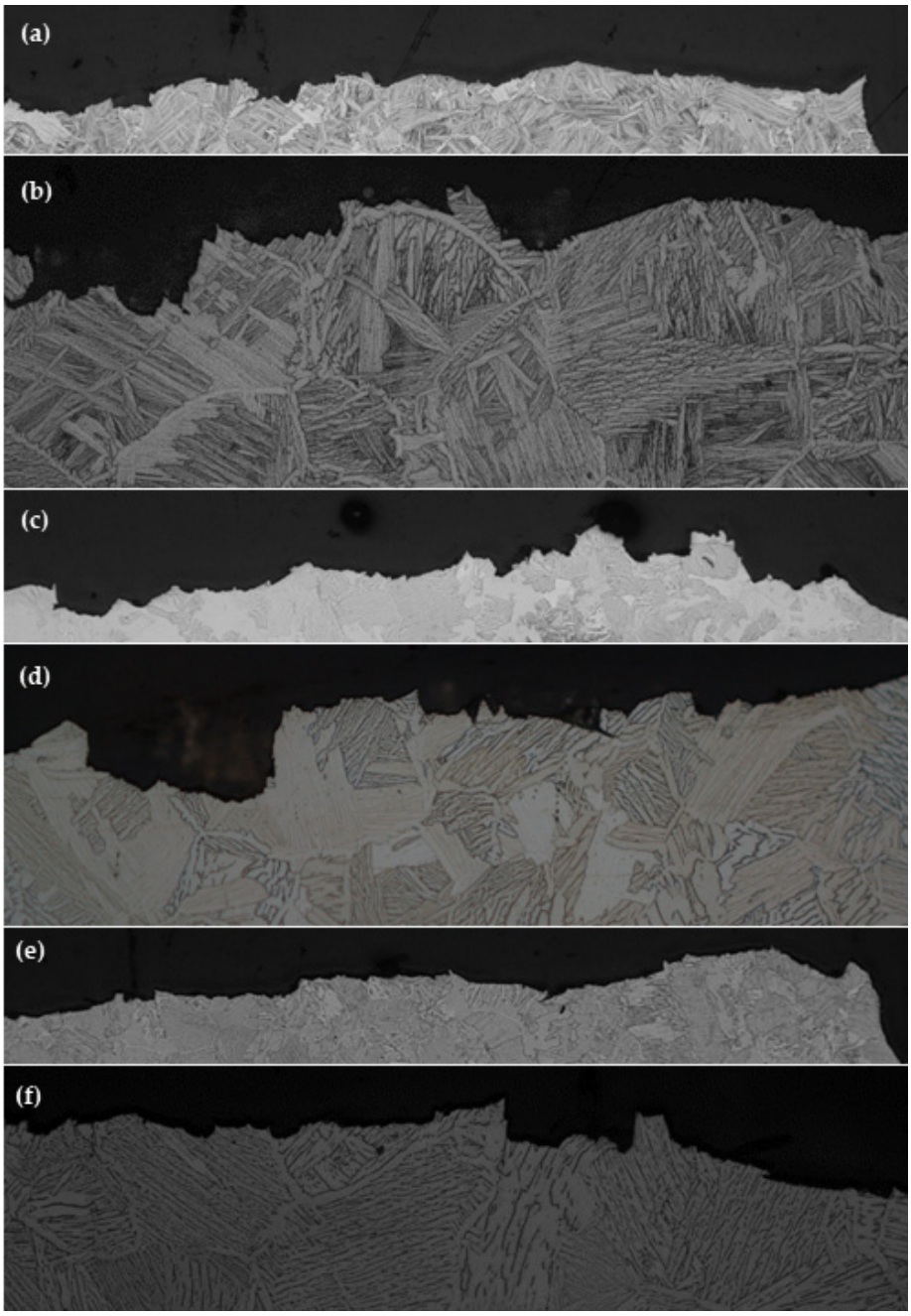

Figure 10. Crack propagation behaviour of impacted specimens (**a**,**b**) as-extruded (**c**,**d**) HT-A (**e**,**f**) HT-B, here images (**a**,**c**,**e**) shows a general appearance and (**b**,**d**,**f**) illustrates the behaviour of the crack within individual grains.

4. Conclusions

In this study, the effect of two sub-transus annealing treatments, HT-A (955 °C/1 h-FC) and HT-B (925 °C/4 h-cooling @ 50 °C/h to 760 °C-FC) on the microstructure and mechanical properties of Ti-6Al-4V alloy developed by TPC-process was investigated. It is apparent that although both sub-transus annealing's have enhanced the tensile strength, but change to ductility was insignificant. Hence the material developed from the TPC route in this study may not be the preferable choice for many structural applications due to its high oxygen content. In as-extruded form, Ti-6Al-4V alloy has an oxygen impurity content of 0.55 wt.% with lamellar microstructure, impact toughness of 4 J, and yield strength around 956 MPa, UTS value around 1150 MPa and a percentage elongation to fracture

of 2.4%. The first sub-transus annealing treatment (HT-A) has given a yield strength of 993 MPa, a UTS of 1181 MPa, a percentage elongation to failure of 3.2%, and impact toughness of 6 J. Similarly, the yield strength, UTS, and ductility after second sub-transus annealing treatment HT-B were reported to be 992 MPa, 1164 MPa, and 2.3% respectively. After HT-B treatment, the impact energy to failure for the samples was around 5 J. An investigation of crack propagation behavior and respective fracture surfaces suggests that a coarsening of the hcp α phase within the β grains and grain boundaries α improved crack propagation resistance, even though transgranular (brittle) fracture was the predominant mode of failure.

Author Contributions: Conceptualization, A.P.S. and B.G.; methodology, A.P.S.; formal analysis, A.P.S. and G.S.; investigation, A.P.S.; resources, B.G.; data curation, A.P.S.; writing—original draft preparation, A.P.S.; writing—review and editing, R.T., G.S. and B.G.; visualization, A.P.S.; supervision, B.G. and R.T.; project administration, B.G.; funding acquisition, B.G. All authors have read and agreed to the published version of the manuscript.

Funding: This research was funded by the Ministry of Business, Innovation, and Employment (MBIE), New Zealand, grant number UOWX1402.

Data Availability Statement: Not applicable.

Acknowledgments: The authors would like to take opportunity to express their great indebtedness to the Titanium Industry Development Association (TiDA) for providing immense technical support for experimental work. The authors' sincere thanks also go to Aamir Mukhtar for the timely support and guidance.

Conflicts of Interest: The authors declare no conflict of interest. Also, the funders had no role in the design of the study; in the collection, analyses, or interpretation of data; in the writing of the manuscript; or in the decision to publish the results.

References

1. International Titanium Association. *Titanium: The Ultimate Choice*; International Titanium Association: Boulder, Colorado, USA, 1999; pp. 1–20.
2. Donachie, M.J. *Titanium: A Technical Guide*, 2nd ed.; ASM International: New York, NY, USA, 2000.
3. Moiseyev, V.N. Applications of Titanium and Titanium Alloys. In *Titanium Alloys: Russian Aircraft and Aerospace Applications*; Taylor & Francis Group: Abingdon, UK, 2006; Volume 5, pp. 195–205.
4. Froes, F.H.S. Titanium Alloys. In *Handbook of Advanced Materials: Enabling New Designs*; Wessel, J.K., Ed.; Wiley-Interscience Publication: New York, NY, USA, 2004; pp. 271–320.
5. Lapovok, R.; Tomus, D. *Production of Dense Compact Billet From Ti-Alloy Powder Using Equal Channel Angular Extrusion*; ARC Centre of Excellence for Design in Light Metals, Dept. of Materials Engineering, Monash University, Clayton: Melbourne, Australia, 2007.
6. Collings, E.W. Powder Metallurgy and Rapid-Solidification Processing. In *Materials Properties Handbook: Titanium Alloys*; Welsch, G., Boyer, R., Collings, E.W., Eds.; ASM International: Materials Park, OH, USA, 1994; pp. 81–86.
7. Froes, F.H.; Eylon, D. *Developments in Titanium P/M*; Institute of Materials & Advanced Processes (IMAP): Moscow, ID, USA, 2005.
8. Abkowitz, S.; Abkowitz, S.; Fisher, H. Breakthrough Claimed for Titanium PM. *Met. Powder Rep.* **2011**, *66*, 16–21. [CrossRef]
9. Qian, M. Cold compaction and sintering of titanium and its alloys for near-net-shape or preform fabrication. *Int. J. Powder Metall.* **2010**, *46*, 29–44.
10. Conway, J.J.; Rizzo, F.J. Hot Isostatic Pressing of Metal Powders. In *Powder Metal Technologies and Applications*; American Society for Metals: Materials Park, OH, USA, 1998; Volume 7, pp. 1425–1462.
11. Moxson, V.S.; Senkov, O.N.; Froes, F.H. Innovations in Titanium Powder Processing. *JOM J. Miner. Met. Mater. Soc.* **2000**, *52*, 24–26. [CrossRef]
12. Abkowitz, S.M.; Abkowitz, S.; Fisher, H.; Main, D.H. Affordable PM titanium—Microstructures, properties and products. In Proceedings of the 2011 International Conference on Powder Metallurgy and Particulate Materials, PowderMet 2011, San Francisco, CA, USA, 24 March 2010.
13. Froes, F.H.; Eylon, D. Powder metallurgy of titanium alloys. *Int. Mater. Rev.* **1990**, *35*, 162–184. [CrossRef]
14. Gabbitas, B.; Yang, F.; Raynova, S.; Jia, M.T. Cost effective forging of titanium alloy parts and their mechanical properties. *Adv. Mater. Res.* **2014**, *1019*, 3–10. [CrossRef]
15. Singh, A.P.; Gabbitas, B.; Torrens, R.; Yang, F.; Mukhtar, A. Mechanical properties of Ti-6Al-4V rods produced by powder compact extrusion. In *TMS 2014: 143rd Annual Meeting & Exhibition*; Springer: Cham, Switzerland, 2014; pp. 605–612.

16. Singh, A.P.; Gabbitas, B.; Yang, F.; Torrens, R. Processing, Microstructure and High Strain Rate Behaviour of Ti-6Al-4V Alloy Produced from a Blended Mixture Using Powder Compact Extrusion. *Key Eng. Mater.* **2016**, *704*, 413–422. [CrossRef]
17. Welsch, G.; Boyer, R.; Collings, E. *Materials Properties Handbook: Titanium Alloys*; ASM international: New York, NY, USA, 1993.
18. Eylon, D.; Froes, F.H.; Abkowitz, S. Titanium powder metallurgy alloys and composites. In *Powder Metal Technologies and Applications (ASM Metals Handbook)*; Lee, P.W., Ferguson, B.L., Eds.; ASM International: Materials Park, OH, USA, 1998; Volume 7, pp. 2192–2231.
19. El-Soudani, S.M. Powder-based titanium alloys: Properties and selection. In *Titanium Powder Metallurgy: Science, Technology and Applications*; Qian, M., Froes, F.H., Eds.; Elsevier: Boston, MA, USA, 2015; pp. 469–496. [CrossRef]
20. Boyer, R.R.; Welsch, G.; Collings, E.W. *Materials Properties Handbook: Titanium Alloys*; ASM International: Materials Park, OH, USA, 1994.
21. Yasa, E.; Deckers, J.; Kruth, J.P.; Rombouts, M.; Luyten, J. Experimental investigation of charpy impact tests on metallic SLM parts. In *Innovative Developments in Design and Manufacturing: Advanced Research in Virtual and Rapid Prototyping*; Bartolo, P.J.D., DeLemos, A.C.S., Pereira, A.M.H., Mateus, A.J.D., Mendes, A.L.A., DeMoura, C.S.M., Capela, C.A.B., DaSilva, C.S.G., Domingues, F.A.C., Bartolo, H., et al., Eds.; CRC: Boca Raton, FL, USA, 2010; pp. 207–214.
22. Wang, L.; Lang, Z.B.; Shi, H.P. Properties and forming process of prealloyed powder metallurgy Ti-6Al-4V alloy. *Trans. Nonferrous Met. Soc. China* **2007**, *17*, s639–s643.
23. Zherebtsov, S.; Kudryavtsev, E.; Kostjuchenko, S.; Malysheva, S.; Salishchev, G. Strength and ductility-related properties of ultrafine grained two-phase titanium alloy produced by warm multiaxial forging. *Mater. Sci. Eng. A Struct. Mater. Prop. Microstruct. Process.* **2012**, *536*, 190–196. [CrossRef]
24. Reda, R.; Nofal, A.; Hussein, A.-H. Effect of single and duplex stage heat treatment on the microstructure and mechanical properties of cast Ti-6Al-4V alloy. *Metallogr. Microstruct. Anal.* **2013**, *2*, 388–393. [CrossRef]
25. Lutjering, G.; Williams, J.C. *Titanium*, 2nd ed.; Springer: Berlin, Germany, 2010; pp. 15–50.
26. Titanium Alloy Guide. Available online: http://rtiintl.s3.amazonaws.com/RTI-Reports/tiguideWeb.pdf (accessed on 4 November 2015).
27. Titanium Ti-6Al-4V (Grade 5), Annealed. Available online: http://asm.matweb.com/search/SpecificMaterial.asp?bassnum=MTP641 (accessed on 4 November 2022).
28. Singh, A.P.; Gabbitas, B.; Yang, F.; Torrens, R.; Mukhtar, A. Effect of Pre-Consolidation Methods and Oxygen on the mechanical Properties of As-Extruded Ti-6Al-4V Alloy Rod. In Proceedings of the 13th World Conference on Titanium, San Diego, CA, USA, 16–20 August 2015; John Wiley & Sons, Inc.: Hoboken, NJ, USA, 2016. [CrossRef]
29. Singh, A.P.; Yang, F.; Torrens, R.; Gabbitas, B. Solution treatment of Ti-6Al-4V alloy produced by consolidating blended powder mixture using a powder compact extrusion route. *Mater. Sci. Eng. A* **2018**, *712*, 157–165. [CrossRef]
30. Singh, A.P.; Yang, F.; Torrens, R.; Gabbitas, B. The effect of heat treatment on the mechanical properties of Ti-6Al-4V alloy produced by consolidating a high impurity blended powder mixture using a combination of powder compact hot pressing and extrusion. *J. Mater. Res.* **2019**, *34*, 1426–1438. [CrossRef]
31. Singh, A.P.; Yang, F.; Torrens, R.; Gabbitas, B. Heat Treatment, Impact Properties, and Fracture Behaviour of Ti-6Al-4V Alloy Produced by Powder Compact Extrusion. *Materials* **2019**, *12*, 3824. [CrossRef] [PubMed]
32. Singh, A.P.; Gabbitas, B.; Brown, I.W.; Mukhtar, A. Processing, microstructure, properties and fracture behaviour of Ti–6Al–4V manufactured from pre-alloyed powder. *Mater. Sci. Technol.* **2021**, *37*, 23–32. [CrossRef]
33. Meyer, L.W.; Krüger, L.; Sommer, K.; Halle, T.; Hockauf, M. Dynamic strength and failure behavior of titanium alloy Ti-6Al-4V for a variation of heat treatments. *Mech. Time-Depend. Mater.* **2008**, *12*, 237–247. [CrossRef]
34. Singh, A.P.; Yang, F.; Torrens, R.; Gabbitas, B.; Robinson, B.; Bolzoni, L. Processing, Microstructures and Properties of a Ti-6Al-4V Extrusion Produced by an Industrial Scale Setup. In *Proceedings of Key Engineering Materials*; Trans Tech Publications: Durnten-Zurich, Switzerland, 2018; Volume 770, pp. 60–69.
35. *ASTM B988-13*; Standard Specification for Powder Metallurgy (PM) Titanium and Titanium Alloy Structural Components. ASTM (American Society for Testing and Materials): West Conshohocken, PA, USA, 2013.
36. Callister, W.D.; Rethwisch, D.G. *Materials Science and Engineering: An Introduction*; Wiley: New York, NY, USA, 2018.
37. Lefebvre, L.P.; Baril, É.; Bureau, M.N. Effect of the oxygen content in solution on the static and cyclic deformation of titanium foams. *J. Mater. Sci. Mater. Med.* **2009**, *20*, 2223–2233. [CrossRef] [PubMed]
38. Wasz, M.L.; Brotzen, F.R.; McLellan, R.B.; Griffin, A.J., Jr. Effect of oxygen and hydrogen on mechanical properties of commercial purity titanium. *Int. Mater. Rev.* **1996**, *41*, 1–12. [CrossRef]
39. Chan, K.S. Relationships of fracture toughness and dislocation mobility in intermetallics. *Metall. Mater. Trans. A* **2003**, *34*, 2315–2328. [CrossRef]